



Determination of low-energy ion-induced electron yields from thin carbon foils

Frédéric Allegrini¹, Robert F. Wimmer-Schweingruber²,
Peter Wurz, Peter Bochsler^{*}

Physikalisches Institut, University of Bern, Sidlerstrasse 5, CH-3012 Bern, Switzerland

Received 4 March 2003; received in revised form 20 May 2003

Abstract

Ion beams crossing thin carbon foils can cause electron emission from the entrance and exit surface. Thin carbon foils are used in various types of time-of-flight (TOF) mass spectrometers to produce start pulses for TOF measurements. The yield of emitted electrons depends, among other parameters, on the energy of the incoming ion and its mass, and it has been experimentally determined for a few projectile elements. The electron emission yield is of great importance for deriving abundance ratios of elements and isotopes in space plasmas using TOF mass spectrometers. We have developed a detector for measuring ion-induced electron yields, and we have extended the electron yield measurements for oxygen to energies relevant for solar wind research. We also present first measurements of the carbon foil electron emission yield for argon and iron in the solar wind energy range.

© 2003 Elsevier B.V. All rights reserved.

PACS: 34.50.Dy; 07.87.+v

Keywords: Ion-induced electron emission; Carbon foil; TOF mass spectrometer

1. Introduction

The interaction of an energetic particle with a solid can lead to electron emission from the sur-

face of the solid. When a projectile passes through a carbon foil, it transfers energy to atoms and electrons within the solid. Outward moving excited foil electrons that are sufficiently close to the surface may have enough energy to escape and to contribute to the electron emission process. When the incident particles are ions, this phenomenon is called ion-induced electron emission (IIEE). A standard parameter describing electron emission is the electron yield, γ , the average number of secondary electrons emitted per primary particle. For comprehensive information on IIEE, see, e.g., reviews by Hofer [1], Rösler and Brauer [2], Hasselkamp [3] and Rothard et al. [4].

^{*} Corresponding author. Tel.: +41-31-631-4429; fax: +41-31-631-4405.

E-mail addresses: fallegrini@swri.edu (F. Allegrini), wimmer@physik.uni-kiel.de (R.F. Wimmer-Schweingruber), peter.wurz@phim.unibe.ch (P. Wurz), bochsler@soho.unibe.ch (P. Bochsler).

¹ Present address: Southwest Research Institute, Instrumentation and Space Research Division, San Antonio, TX, USA.

² Present address: Institut für Experimentelle und Angewandte Physik, Universität Kiel, Germany.

To first approximation, the electron yield is proportional to the electronic stopping power $S_e = (dE/dx)_e$:

$$\gamma \cong A \cdot S_e / \cos \alpha, \quad (1)$$

where A is the constant of proportionality (sometimes called the specific yield), and α is the angle of incidence of the projectile with respect to the surface normal [5–8]. Deviations from the above formula are expected and observed at low energies [see e.g., 8] and at large angles of incidence [9]. For the following it is important that the electron emission yield depends specifically on the local stopping power (i.e. the electronic stopping power of the projectile near the emitting surface of the solid) and not on the travelled distance within the solid nor on the total energy deposited by the projectile.

The time-of-flight (TOF) technique is a well established technique for determining the ion composition of space plasmas (see reviews by Young [10] and Wüest [11]). In TOF mass spectrometers designed for low particle energies (\sim keV/amu) often very thin ($\sim 2 \mu\text{g}/\text{cm}^2$) carbon foils are used. When a particle passes through the carbon foil, electrons are emitted from both, the entrance and the exit surfaces. The emitted electrons are then collected by a micro-channel plate (MCP) assembly, which produces a start pulse for the TOF measurement. When the number of emitted electrons is low, the probability, η , of triggering a signal on the MCP is a strong function of this number (typically $\eta = 1 - e^{-p\gamma}$ where p is the MCP detection efficiency for a single electron). The value of γ is thus crucial for the determination of instrument detection efficiencies.

The energy range of solar wind particles extends typically from 0.3 to 4 keV/amu. In this range, electron emission yields from thin carbon foils have only been reported for a few projectile elements (from H to Ne) by Ritzau and Baragiola [12], (C, N, O, Ne) by Keller et al. [13], (O) by Kerkow et al. [14] and (O, S) by Kozochkina et al. [15]. In the solar wind also many other elements have been detected such as, e.g., Na, Mg, Al, Si, Cl, Ar, Ca and Fe, yet no experimental data for electron emission yields of such projectiles are available in the energy range of interest.

2. Experimental setup

Fig. 1 shows the schematics of our experiment. The ion beam enters the pinhole (diameter 3 mm) from the left, and passes through the carbon foil, where the electron emission takes place. The outgoing particles (mainly neutrals at solar wind energies) are then collected by the Faraday cup, whereas the electrons are collected by the backward and forward cups. The electrodes on each side of the cups are kept at negative potentials to force the electrons toward the cups. The cups themselves are kept at a positive potential. I_b is the current of the backward emitted secondary electrons, I_c is the current measured at the carbon foil, I_f is the current of the forward emitted secondary electrons and I_t is the current measured with the Faraday cup.

The ion beam was produced with a 2.45 GHz ECR ion source [16,17], which was developed to test and to calibrate mass spectrometers for space research. Only beams of weakly ionized species were used for this work.

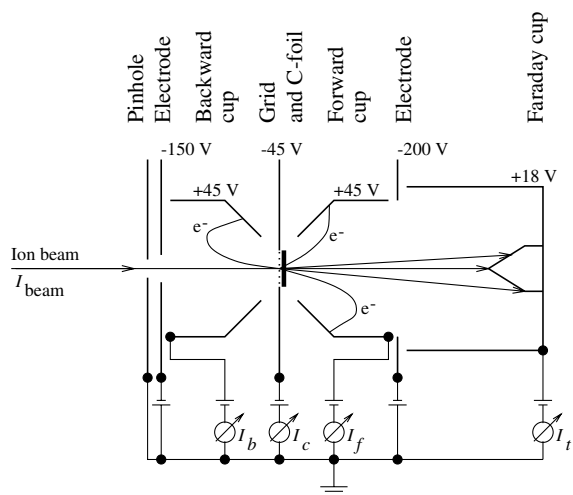


Fig. 1. Schematics of the experiment. The backward and forward cups are kept at a positive potential (+45 V), whereas the electrodes on both sides of the foil complex are kept at negative potentials. Secondary electrons emitted from the carbon foil (at -45 V) are accelerated away from the foil and then attracted by the cups. The carbon foil is usually mounted on the downstream side of a 83% transmission nickel grid.

Since the foils are too thin to stand free in an aperture of 8.5 mm, they must be mounted on thin nickel grids. The transmission of the grids was measured, both, optically and with an ion beam. From both measurements we obtain a transmission of $(83 \pm 1)\%$.

The carbon foils were purchased from Arizona Foil Company (AFC). According to specifications of this manufacturer, the uncertainty of the thickness is $\pm 0.2 \mu\text{g}/\text{cm}^2$ for foils with a thickness below a nominal value of $5 \mu\text{g}/\text{cm}^2$. Above a nominal value of $5 \mu\text{g}/\text{cm}^2$ the quoted thickness uncertainty is $\pm 5\%$. However, these specifications might be overly optimistic for thin AFC foils. Apparently, thin AFC foils could be as much as 50% thicker than the given specifications. The nominal density of a $20 \mu\text{g}/\text{cm}^2$ carbon foils is $2.01 \pm 0.02 \text{ g}/\text{cm}^3$ according to the manufacturer [18]. Ritzau and Baragiola [12] found a similar value of $1.8 \text{ g}/\text{cm}^3$ for carbon foils of $0.5 \mu\text{g}/\text{cm}^2$.

The foil holder can carry as many as five different carbon foils. In addition, it is possible to mount an empty grid. Hence, this allows to measure the beam current, and to derive the contribution of the grid to the electron emission.

The secondary electron yield γ is defined as the ratio of the number of emitted electrons to the number of incoming particles. Determining the electron yield from carbon foils requires distinguishing electrons emitted from the foil from those, which are emitted from the grid. Hence, in order to derive the net electron emission one has to measure the difference between a bulk current emitted from a grid carrying a carbon foil (superscript 2), and a grid without foil (superscript 1). To calculate the yield, one relates this difference to the number of incoming particles, which is identical to the number of particles that have passed the grid, since the grid is upstream with respect to the carbon foil, and all particles passing the foil have to pass the grid. The flux of particles passing the grid is derived from the current measured after a grid without carbon foil ($I_t^{(1)}$). Secondary electron currents in the forward direction and the backward directions are denoted with subscripts f and b, respectively. The backward electron yield is then obtained from

$$\gamma_b = -\frac{I_b^{(2)} - I_b^{(1)}}{I_t^{(1)}/q}, \quad (2)$$

where q is the charge of the incoming particles. Similarly, the forward yield is given by

$$\gamma_f = -\frac{I_f^{(2)} - I_f^{(1)}}{I_t^{(1)}/q}. \quad (3)$$

The negative signs in the above equations account for the fact that the emitted particles are electrons, thus the currents are negative. We also measure $I_t^{(2)}$, which is the current of particles that have undergone charge exchange while passing the foil. The charge exchange process has been extensively investigated by Gonin et al. [19] and Kallenbach et al. [20], who give an algorithm to calculate charge exchange yields at given incident energies for many elements, thus allowing a comparison of $I_t^{(2)}$ with their measurements.

With this configuration, one cannot detect the so-called delta electrons, which result from close collisions with near-surface atoms. They are too energetic ($E > 50 \text{ eV}$), and the potentials used in our setup are too low to deflect their trajectories toward the collecting cups. In any case, at the low projectile energies considered here, delta electrons represent a small fraction of the electron emission [21] and we neglect this contribution in this work. Note, that the backward yield also depends on the charge state of the incoming ions if these are highly charged. The measurements presented here have been obtained with weakly (singly or doubly) charged particles.

Impurities on the surface of a carbon foil generally lead to an increase in the electron yield. The impurities can be removed by sputter cleaning, e.g., by means of bombarding the foil with rare gas ions [3,8,12,22]. Fig. 2 illustrates the effect of sputter cleaning on the electron yields. The yields are given as a function of the total particle fluence. The error bars in Fig. 2 have been derived from the standard deviations of fluctuating current measurements. The experimental uncertainties are often smaller than the symbols. To clean the foil, for which the yields are shown in Fig. 2, we used argon ions with $1 \text{ keV}/\text{amu}$. The current density never exceeded $30 \text{ pA}/\text{mm}^2$. The electron yields clearly

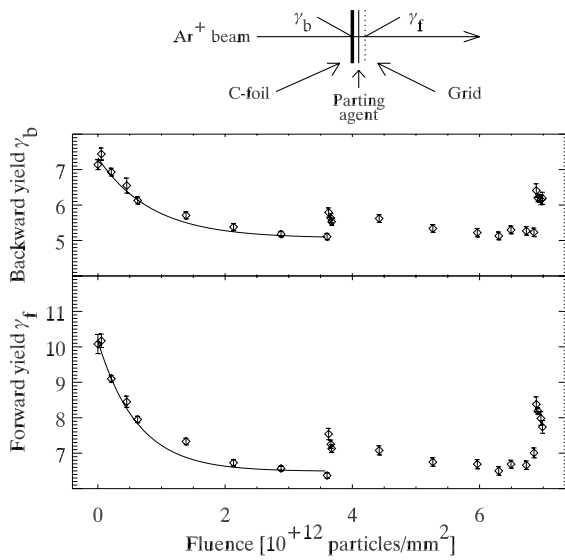


Fig. 2. Electron yields during cleaning of a $2.1 \mu\text{g}/\text{cm}^2$ carbon foil with Ar^+ at 1 keV/amu. The fluence corresponds to the number of argon ions that hit the foil. For this experiment the foil was exceptionally mounted upstream with respect to the grid.

decrease with fluence; the thin line is a fit to the data using the function

$$\gamma_i = a_i + b_i \cdot e^{-c_i F}, \quad (4)$$

where a_i , b_i and c_i are the fitting parameters, F is the fluence and the subscript “i” refers to the backward (b) and forward (f) yields, respectively. F is given in particles/ nm^2 . The parameter a_i is interpreted as the clean foil yield obtained, once most of the impurities have been removed (Table 1).

For the sputter experiment, the foil had been mounted upstream with respect to the grid (contrary to what was stated in the discussion of Eqs. (2) and (3)). As a consequence, the detergent (parting agent) used to separate the carbon foil from the glass plate, on which it was originally

deposited, is on the forward surface. Eq. (4) describes the effect of the sputter treatment. In this context the parameter c can be considered as the sputtering cross section of a “dirt” particle against removal by an argon ion. The exponential decay of the contaminant yield (b) is ascribed to the fact that the probability of a projectile hitting a dirt particle decreases with increasing fluence.

The conspicuous discontinuities in the secondary electron yields in Fig. 2 correspond to interruptions of the sputter treatment. The first interruption lasted 16 h, with the carbon foil kept under vacuum conditions at a pressure of $7 \cdot 10^{-8}$ mbar. Apparently the contamination layer had partly recovered during the break of the treatment. Interestingly, after resuming the sputter process, the electron yield of the contamination layer decayed much more rapidly at the beginning, indicating that the newly formed contamination layer was more volatile than the original contamination layer. According to Caron et al. [23] this contamination must probably be attributed to a nitrogen and/or oxygen layer covering the foil, and not (contrary to our expectation) to a water skin. Considering the more sluggish decay of a second contribution of the electron yield, a less volatile contamination layer seems also present, which we tentatively attribute to hydrocarbons, either derived from the detergent, or newly formed, via the interaction of hydrogen with the foil.

3. Projectile dependent electron yields

Measurements of the backward and forward yields were performed for different thicknesses of carbon foils: 1.5, 2.1, 2.5, 3.6, 4.5 and $10 \mu\text{g}/\text{cm}^2$ (nominal values). We did not measure the foil thicknesses. Gonin [24, p. 51] reported a thickness uncertainty of $\sim 15\%$ for the foils provided by AFC. He also mentions references reporting much larger uncertainties [see e.g., 25,26].

In Figs. 3–5 we show the secondary electron yields for oxygen, argon and iron, respectively. The yields for oxygen are compared with results from the literature (filled symbols). Our measurements (open symbols) are consistent with values published by other authors. We have extended

Table 1

Parameters for describing the variation of electron yields with particle fluence in Eq. (4)

	a [nm^2]	b [nm^2]	c [nm^2]
Backward electron yield	5.1	2.3	1.2
Forward electron yield	6.5	3.7	1.6

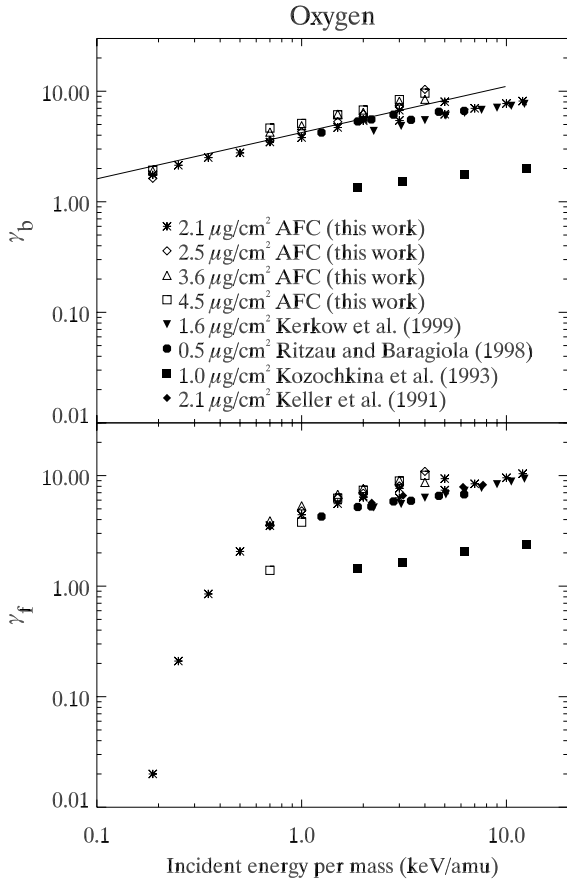


Fig. 3. Measured backward and forward yields for oxygen compared with the literature. The open symbols represents our measurements done with the foils from Arizona Foil Company (AFC) and the filled ones data from (▼) Kerkow et al. [14], (●) Ritzau and Baragiola [12], (■) Kozochkina et al. [15] and (◆) Keller et al. [13].

these measurements to lower energies. At such energies and as discussed in the previous section, the foil contamination plays an important role for the electron yields. Despite the fact that our foils were cleaned by sputtering, contaminants have probably resisted and this could partly explain the spread of our measurements. The yields for iron ions are, to our knowledge, the first measurements of the electron yields for this element in the keV/amu solar wind energy range.

The thin lines in the upper panels of Figs. 3–5 fit our measurements of the backward yield according to the function

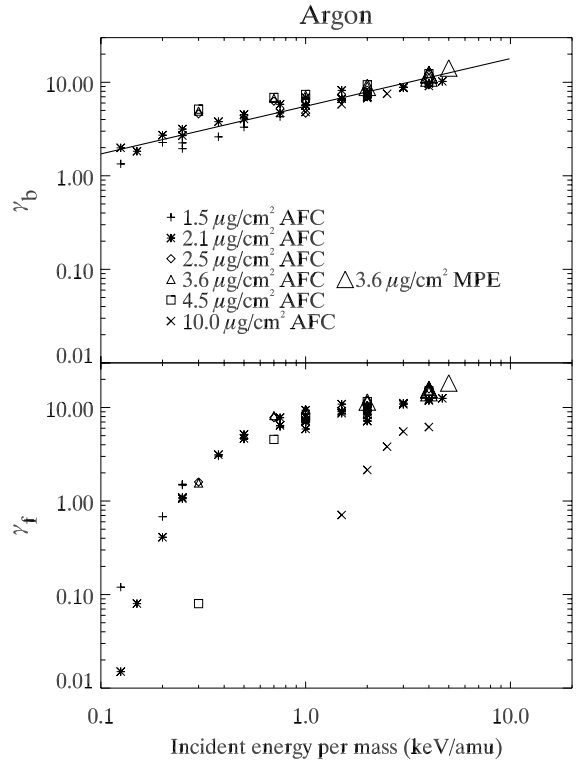


Fig. 4. Measured backward and forward yields for argon. The symbols correspond to the following thicknesses: (+) 1.5 $\mu\text{g}/\text{cm}^2$, (*) 2.1 $\mu\text{g}/\text{cm}^2$, (◇) 2.5 $\mu\text{g}/\text{cm}^2$, (△) 3.6 $\mu\text{g}/\text{cm}^2$, (□) 4.5 $\mu\text{g}/\text{cm}^2$, (×) 10.0 $\mu\text{g}/\text{cm}^2$. The foils were purchased from Arizona Foil Company except for one 3.6 $\mu\text{g}/\text{cm}^2$ sample (symbol △), which was provided by the Max Planck Institute for Extraterrestrial Physics in Garching, Germany (MPE).

$$\log \gamma_b = \log A_b + k_E \log \frac{E_i}{m}, \quad (5)$$

which is equivalent to Eq. (1) ($\gamma \propto S_e$) assuming electronic stopping $S_e \propto v^{k_v} \propto (\frac{E}{m})^{k_E}$ (LSS theory [27]) where $k_v \approx 1$ and $k_E \approx 0.5$. For oxygen we find $k_E = 0.42$, for argon $k_E = 0.50$ and for iron $k_E = 0.75$. The fits confirm the general power-law dependence of electron yields on energy per mass, and hence, on the electronic stopping power.

Note that the plots in Figs. 3–5 show electron yields versus *incident* particle energy, as this is the relevant parameter for our application. A decrease of efficiency is observed when the projectile velocity drops below the required threshold to

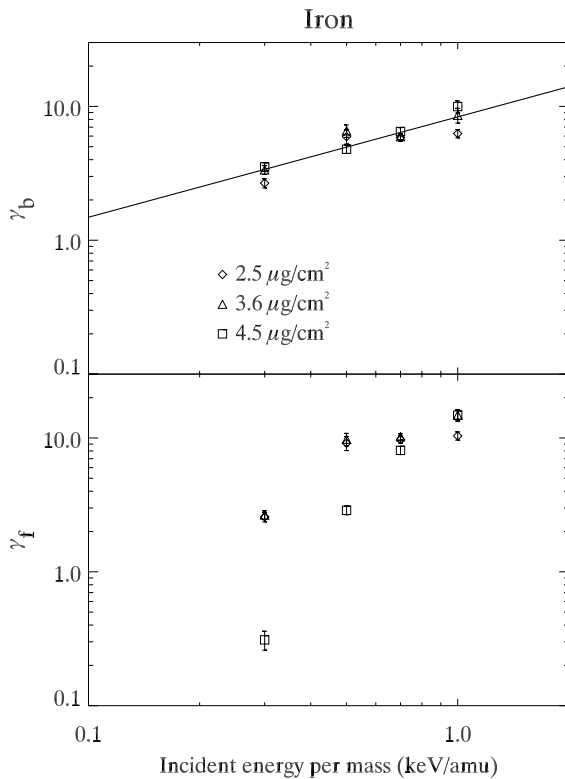


Fig. 5. Measured backward and forward yields for iron.

transfer sufficient momentum to the conducting electrons to escape through the surface potential. At even lower energies many projectile ions no longer pass the foils and the forward yield begins to strongly depend on the amount of crossing projectiles. As a consequence the forward yield drops dramatically at low incident energies.

4. Forward to backward electron yield ratio

Fig. 6 illustrates the forward–backward ratio of the electron yield as a function of incident ion energy. It is roughly constant above 1 keV/amu for 2.1 $\mu\text{g}/\text{cm}^2$ and drops toward lower energies. For thinner foils γ_f/γ_b drops at lower energies than it does for thicker foils. This is an expected consequence of the inability of low energy ions to emit electrons at the exit or even to reach the exit sur-

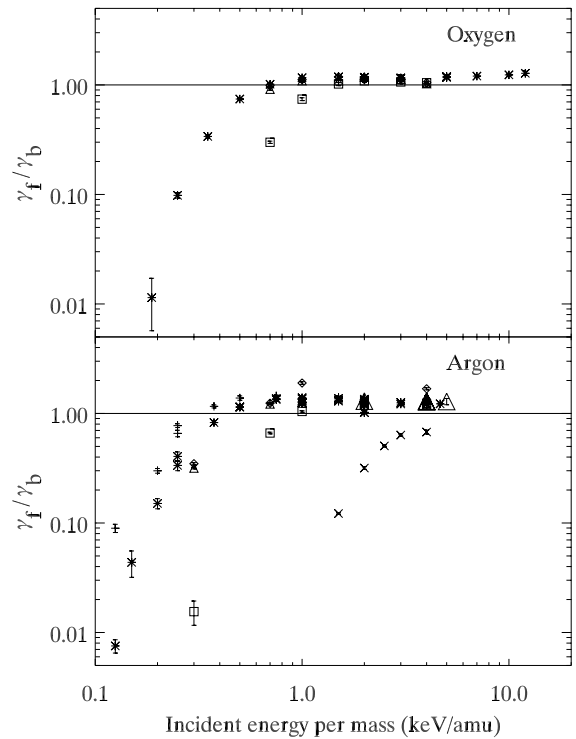


Fig. 6. Ratio of forward to backward yields for oxygen (upper panel) and argon (lower panel). The symbols correspond to the following thicknesses: (+) 1.5 $\mu\text{g}/\text{cm}^2$, (\ast) 2.1 $\mu\text{g}/\text{cm}^2$, (\diamond) 2.5 $\mu\text{g}/\text{cm}^2$, (\triangle) 3.6 $\mu\text{g}/\text{cm}^2$, (\square) 4.5 $\mu\text{g}/\text{cm}^2$, (\times) 10.0 $\mu\text{g}/\text{cm}^2$. Experimental uncertainties are only indicated with error bars for cases, in which the estimated uncertainty is larger than the symbol.

face. Typical ranges of oxygen ions at 1 keV/amu incident energy are of the order of 5 $\mu\text{g}/\text{cm}^2$, hence it is no surprise to see the loss of forward emission capability at approximately 1 keV/amu for foils of 4.5 $\mu\text{g}/\text{cm}^2$. Argon ions with 1 keV/amu have a somewhat wider range of 8 $\mu\text{g}/\text{cm}^2$ within carbon foils. The drop in forward emission, however, begins already at a somewhat higher energy, possibly because the momentum transfer to electrons is insufficient to emit an electron, although the projectile still passes the foil. Furthermore, at low energies the projectiles tend to neutralize, thus reducing the electronic stopping power and simultaneously reducing the electron emission efficiency again.

The ratio γ_f/γ_b at higher energies is constant, confirming the general validity of the basic rule of Sternglass [5] given in Eq. (1) for forward as well as for backward yields. The forward yield somewhat exceeds the backward yield, despite the particle energy being lower at the exit, we thus confirm that $A_f > A_b$ in the low energy range, consistent with observations at higher energies [8,28].

5. Conclusion

We have measured ion-induced electron yields from thin carbon foils such as used in space instrumentation. We have presented the first measurements of the forward and backward electron yields for argon and iron in the solar wind energy range (0.3–4 keV/amu). We also have measured oxygen electron yields at lower energies than previously reported in the literature. In the high energy range ($E/m > 1$ keV/amu) our measurements agree with values found in the literature.

We have verified the power law dependence between the backward electron yield and the incident energy. The power law is consistent with the hypothesis of a proportionality between the yield and the electronic stopping power, even at the low energies reported here.

We also find that contamination of thin foils can have a noticeable influence on the electron emission properties. Furthermore, contamination can lead to a systematic overestimation of thicknesses of thin foils. These effects do not hamper the application of such foils for space research, as long as they are carefully taken into account for data evaluation and interpretation. Although the set of electron yield parameters, determined experimentally at low energies is still limited, it constitutes a useful database for extrapolation of experimental data from higher energies to solar wind energies. In space applications this is especially helpful for determining high precision elemental abundance ratios of space plasmas for elements with properties, which do not differ too much in mass.

Acknowledgements

The authors are grateful to Markus Hohl for his invaluable help with the Mefisto ion source and to Martin Wieser for improvements of the current experimental setup. Many thanks also to Hermann Rothard for his good advice and to an anonymous referee for numerous helpful comments. This work was supported by the Swiss National Foundation.

References

- [1] W.O. Hofer, *Scanning Microsc.* 4 (Suppl.) (1990) 265.
- [2] M. Rösler, W. Brauer, in: G. Höhler (Ed.), *Particle Induced Electron Emission I*, Springer-Verlag, Berlin, 1991, p. 1.
- [3] D. Hasselkamp, in: G. Höhler (Ed.), *Particle Induced Electron Emission II*, Springer-Verlag, Berlin, 1992, p. 1.
- [4] H. Rothard, K.O. Groeneveld, J. Kemmler, in: G. Höhler (Ed.), *Particle Induced Electron Emission II*, Springer-Verlag, Berlin, 1992, p. 97.
- [5] E.J. Sternglass, *Phys. Rev.* 108 (1957) 1.
- [6] J. Schou, *Phys. Rev. B* 22 (1980) 2141.
- [7] R.A. Baragiola, E.V. Alonso, A.O. Florio, *Phys. Rev. B* 19 (1979) 121.
- [8] H. Rothard, K. Kroneberger, A. Clouvas, E. Veje, P. Lorenzen, N. Keller, J. Kemmler, W. Meckbach, K.-O. Groeneveld, *Phys. Rev. A* 41 (1990) 2521.
- [9] R.A. Baragiola, *Phys. Rev. B* 78 (1993) 223.
- [10] D.T. Young, in: J.H. Waite, Jr., J.L. Burch, R.L. Moore (Eds.), *Solar System Plasma Physics*, AGU Monogr. Ser., Vol. 54, 1989, p. 143.
- [11] M. Wüest, in: R.F. Pfaff, J.E. Borovsky, D.T. Young (Eds.), *Measurement Techniques in Space Plasmas: Particles*, AGU Monogr. Ser., Vol. 102, 1998, p. 141.
- [12] S.M. Ritzau, R.A. Baragiola, *Phys. Rev. B* 58 (1998) 2529.
- [13] J.W. Keller, K.W. Ogilvie, J.W. Boring, R.W. McKennie, *Nucl. Instr. and Meth. B* 61 (1991) 291.
- [14] H. Kerkow, R. Stolle, V.P. Petukhov, E.A. Romanovskii, *Nucl. Instr. and Meth. B* 154 (1999) 330.
- [15] A.A. Kozochkina, V.B. Leonas, V.E. Fine, in: R.A. Baragiola (Ed.), *Ionization of Solids by Heavy Particles*, Plenum Press, New York, USA, 1993, p. 223.
- [16] A. Marti, R. Schletti, P. Wurz, P. Bochsler, *Rev. Sci. Instr.* 72 (2) (2001) 1354.
- [17] M. Hohl, Ph.D. thesis, University of Bern, Switzerland, 2002.
- [18] J.O. Stoner Jr., *Nucl. Instr. and Meth. A* 303 (1991) 94.
- [19] M. Gonin, R. Kallenbach, P. Bochsler, *Nucl. Instr. and Meth. B* 94 (1994) 15.
- [20] R. Kallenbach, M. Gonin, P. Bochsler, A. Bürgi, *Nucl. Instr. and Meth. B* 103 (1995) 111.
- [21] D. Hasselkamp, S. Hippler, A. Scharmann, *Nucl. Instr. and Meth. B* 18 (1987) 561.

- [22] H. Rothard, M. Jung, B. Gervais, J. Grandin, A. Billebaud, R. Wünsch, *Nucl. Instr. and Meth. B* 107 (1996) 108.
- [23] M. Caron, F. Haranger, H. Rothard, B. Ban d'Etat, P. Boduch, A. Clouvas, C. Potiriadis, R. Neugebauer, T. Jalowy, *Nucl. Instr. and Meth. B* 179 (2001) 167.
- [24] M. Gonin, Master's thesis, University of Bern, Switzerland, 1991.
- [25] W. Stüdemann, B. Wilken, *Rev. Sci. Instr.* 53 (1982) 175.
- [26] G. Both, E.P. Kanter, Z. Vager, B.J. Zabransky, D. Zajfman, *Rev. Sci. Instr.* 58 (1987) 424.
- [27] J. Lindhard, M. Scharff, H.E. Schiøtt, *Mat. Fys. Medd. Dan. Vid. Selsk.* 33 (1963) 14.
- [28] A. Clouvas, C. Potiriadis, H. Rothard, D. Hofmann, R. Wünsch, K.O. Groeneveld, A. Katsanos, A.C. Xenoulis, *Phys. Rev. B* 55 (1997) 12086.